

Constructing a Resilient Hierarchical Conductive Network to Promote Cycling Stability of SiO_x Anode via Binder Design

Zhibo Song, Shiming Chen, Yan Zhao,* Shida Xue, Guoyu Qian, Jianjun Fang, Taohang Zhang, Chuanjiang Long, Luyi Yang,* and Feng Pan*

Despite exhibiting high specific capacities, Si-based anode materials suffer from poor cycle life as their volume change leads to the collapse of conductive network within the electrode. For this reason, the challenge lies in retaining the conductive network during electrochemical processes. Herein, to address this prominent issue, a cross-linked conductive binder (CCB) is designed for commercially available silicon oxides (SiO_x) anode to construct a resilient hierarchical conductive network from two aspects: on the one hand, exhibiting high electronic conductivity, CCB serves as an adaptive secondary conductive network in addition to the stiff primary conductive network (e.g., conductive carbon), facilitating faster interfacial charge transfer processes for SiO, in molecular level; on the other hand, the cross-linked structure of CCB shows resilient mechanical properties, which maintains the integrity of the primary conductive network by preventing electrode deformation during prolonged cycling. With the aid of CCB, untreated micro-sized SiO, anode material delivers an areal capacity of 2.1 mAh cm⁻² after 250 cycles at 0.8 A g⁻¹. The binder design strategy, as well as, the relevant concepts proposed herein, provide a new perspective toward promoting the cycling stability of highcapacity Si-based anodes.

1. Introduction

To fulfill the demands of next-generation lithium-ion batteries (LIBs), advanced electrode materials have been extensively developed.^[1–4] Owing to its high specific capacity (4200 mAh g^{−1}), Si has been regarded as one of the most promising alternatives to replace commercially used graphite anode.^[5] However, the vast volume fluctuation of Si (≈400%) during lithiation/delithiation

Z. Song, S. Chen, S. Xue, G. Qian, J. Fang, T. Zhang, L. Yang, F. Pan School of Advanced Materials Peking University Shenzhen Graduate School Shenzhen 518055, P. R. China

E-mail: yangly@pkusz.edu.cn; panfeng@pkusz.edu.cn

Y. Zhao

Department of Mechanical Engineering Imperial College London London SW7 2BX, UK E-mail: yan.zhao@imperial.ac.uk

C. Long

Department of Materials Science and Engineering National University of Singapore Singapore 117575, Singapore

(D)

The ORCID identification number(s) for the author(s) of this article can be found under https://doi.org/10.1002/smll.202102256.

DOI: 10.1002/smll.202102256

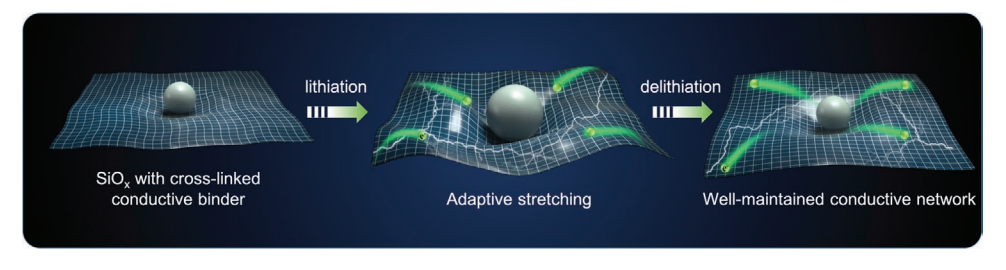
and the costly production of nanostructured Si seriously impeded the extensive application. $^{[6,7]}$ Recently, silicon oxides (SiO_x) has been considered as a competitive substitute for elemental Si owing to its low cost, facile synthesis, and improved cycling stability. $^{[8-11]}$ As a result, SiO_x has been used in a blended form with graphite (with a restricted content) and adopted in commercialized LIBs. $^{[12,13]}$ Nevertheless, the long-term cycling of SiO_x is still hindered by its intrinsically inferior conductivity and non-negligible volume change. $^{[8]}$

As the result of repeated expansion and contraction, the failure of SiO_x anode is generally attributed to the collapse of the conductive network, which mainly consists of carbon-based additives. However, most carbon additives have very weak physical contact interactions with active materials, hence unable to tolerate drastic volume changes. Therefore, one of the most emergent challenges for SiO_x anodes is to retain their conductive networks. To

address this prominent issue, two approaches can be adapted:
1) Mechanically constraining the fracture of the electrode;
2) extending the conductive network within the electrode.

Binders play crucial roles in LIBs to boost battery performance by holding critical components of electrodes, such as active materials, conductive additives, and current collectors, firmly together during charge/discharge processes. The development and application of multifunctional binders mainly aim to improve the adhesion force and the mechanical strength. Kohzo Konno et al.[14] showed that the electrochemical activity of the SiO_x composite electrode is significantly improved by using poly(acrylic acid) (PAA) compared to conventional poly(vinylidene fluoride), poly(vinyl alcohol), and carboxymethyl cellulose sodium (CMC) as the abundant -COOH polar groups in PAA chains can provide sufficient adhesive force to SiO_x particles. Choi et al. further prepared a pyrene-PAA-polyrotaxane supramolecular network, effectively buffering the volume expansion of SiO_x and largely mitigating the electrode swelling.[15] Junmin Nan et al. developed three-dimensional rigidity-reinforced SiO_x anodes using the multicomponent binder.^[16] Lin et al. utilized a three-in-one design strategy to prepare all-integrated SiOx anode with high mass loading.[17] However, simply tuning mechanical properties of binders cannot fully address the existing issues as nonconductive binders are unable to perform as a well-connected electron transport network between active materials.

16136829, 2021, 42, Downloaded from https://onlinelbtary.wiley.com/doi/10.1002/snlll.20210256 by University Town Of Shenzhen, Wiley Online Library on [26111025]. See the Terms and Conditions (https://onlinelibrary.wiley.com/terms-and-onditions) on Wiley Online Library for rules of use; OA articles are governed by the applicable Creative Commons Licenses



Scheme 1. Schematic illustration of interaction between the SiO_x pariticle and the resilient conducive network during lithiation/delithation processes.

Alternatively, serving simultaneously as binding and conducting agents, conductive binders provide tributaries of current flow at the molecular level around the surface of semi-conductive Si-based materials owing to their adaptivity and good conductivity. By extending the primary (long-range) electron conduction network, a secondary (short-range) conductive network is constructed at the interface of active materials. Through a larger electronic contact area, this hierarchical conductive network facilitates to reduce the overall electronic resistance of electrodes, especially when the "point contact" between the stiff primary conductive network and active materials is disrupted by the volume changes.^[18] Consequently PFFOMB,^[19] PPy,^[20] PEDOT:PSS, [21] PFM, [22,23] PF-COONa, [24] PFPO-COONa, [25] etc., have been explored to build secondary conductive network for Si-based anodes.

Although these conductive binders can effectively improve the electron conduction in Si-based anodes, their applications are hindered by the deficiency of mechanical strength. Polymer chains in linear conductive binder (LCB) only have relatively weak interactions (e.g., Van der Waals' force and hydrogen bonding), which cannot buffer the frequent expansion and shrinkage of micro-sized silicon-based particles, leading to the disintegration of the electrode. Therefore, it is crucial to design novel conductive binders that possess robust mechanical properties for micro-sized SiO_x electrodes. It has been previously demonstrated that cross-linking could be an effective approach to promote the mechanical strength of binders as the constructed 3D networks could better adapt to the drastic volume changes.[26-32] Herein, we have designed and synthesized a polyfluorene-type cross-linked conductive binder (CCB) by connecting LCBs onto conjugated anchor points through covalent bonds, which not only has a remarkable intrinsic conductivity to serve as the secondary conductive network, but also exhibits excellent mechanical properties to preserve the network (shown in Scheme 1). Consequently, a robust hierarchical conducting network is constructed for micro-sized SiO_x anodes which is potentially beneficial for both the rate capability and the longterm cycling stability.

2. Results and Discussion

The chemical structure and synthesis of the novel CCB denoted as CCB is schematically demonstrated in Figure 1a and Figure S1, Supporting Information, respectively. The condensation polymerization was carried out using the Suzuki coupling reaction, after which the obtained polymer was acid-hydrolyzed and subsequently neutralized by extra sodium hydroxide to

gain the water-soluble CCB. Due to the existence of M3 among the monomers, the structure of CCB can be seen as covalently bonded LCB polymer chains through conjugated anchor points (i.e., triphenyl benzene). Since the main difference between CCB and LCB is the additional triphenyl benzene segments, Fourier transform infrared (FTIR) spectra (Figure S2, Supporting Information) and Raman spectra (Figure S3, Supporting Information) of CCB and LCB are almost identical as expected.^[24,33,34] In spite of the similar functional groups exhibited by CCB and LCB, the cross-linking structure dramatically improves the mechanical strength of the polymer. The viscosity of the 1.5 wt% CCB solution is obviously higher than the 1.5 wt% LCB solution owing to the existence of cross-linked network in CCB (Figure S4, Supporting Information). To evaluate the effectiveness of cross-linking, the nanoindentation was used to measure the mechanical properties of the polymer films. As shown in Figure 1b, the CCB film exhibits higher Young's modulus and hardness than the LCB film, which are essential to maintain the integrity of SiO_x electrodes. For comparison purpose, mechanical properties of PAA and CMC are also tested as benchmarking groups (Figures S5 and S6, Supporting Information). CCB with 5% molar ratio of M3 in monomers can lead to a moderate mechanical strength which is between LCB and PAA. It is worth mentioning that the moderate Young's modulus of CCB keep a reasonable level upon mild deformation, which means that the CCB matrix in the SiO_x electrodes can buffer the volume expansion of SiO_x to a certain extent. Additionally, the Young's modulus of CCB increases after the deformation is beyond a certain limit which would help restrain the collapse of the electrodes during cycling. These mechanical properties are mainly related to the degree of cross-linking which can be further tuned by changing the molar ratio of monomers. Moreover, adequate mechanical strength is essential for SiO_x electrodes especially for micro-sized SiO_x as shown in Figure S7, Supporting Information. To evaluate the influence of binders on the adhesion force of SiO_x electrodes, peeling tests of SiO_x/LCB, SiO_x/CMC, SiO_x/PAA, and SiO_x/CCB electrodes were performed. As shown in Figure 1c, the adhesion force of SiO_x/PAA and SiO_x/CCB are much greater than SiO_x/LCB and SiO_x/CMC (raw data are shown in Figure S8, Supporting Information). This result can be attributed to the abundant anchor points in cross-linked CCB which effectively reduce the mobility of polymer chains. According to our previous work, chemical bonding can be formed between LCB and Si-based particles which is believed to boost the adhesive force. [24] The chemical bonds between the carboxylic groups of CCB and the hydroxyl groups of the SiO_x particles can be directly identified by FTIR spectroscopy (Figure S9, Supporting Information). A new band

16136829, 2021, 42, Downloaded from https:/

/onlineliblary.wiley.com/doi/10.1002/smll.02102256 by University Town Of Shenzhen, Wiley Online Library on [26/11/2025]. See the Terms and Conditions (https://onlinelibrary.wiley.com/terms-and-conditions) on Wiley Online Library for rules of use; OA articles are governed by the applicable Creative Commons License

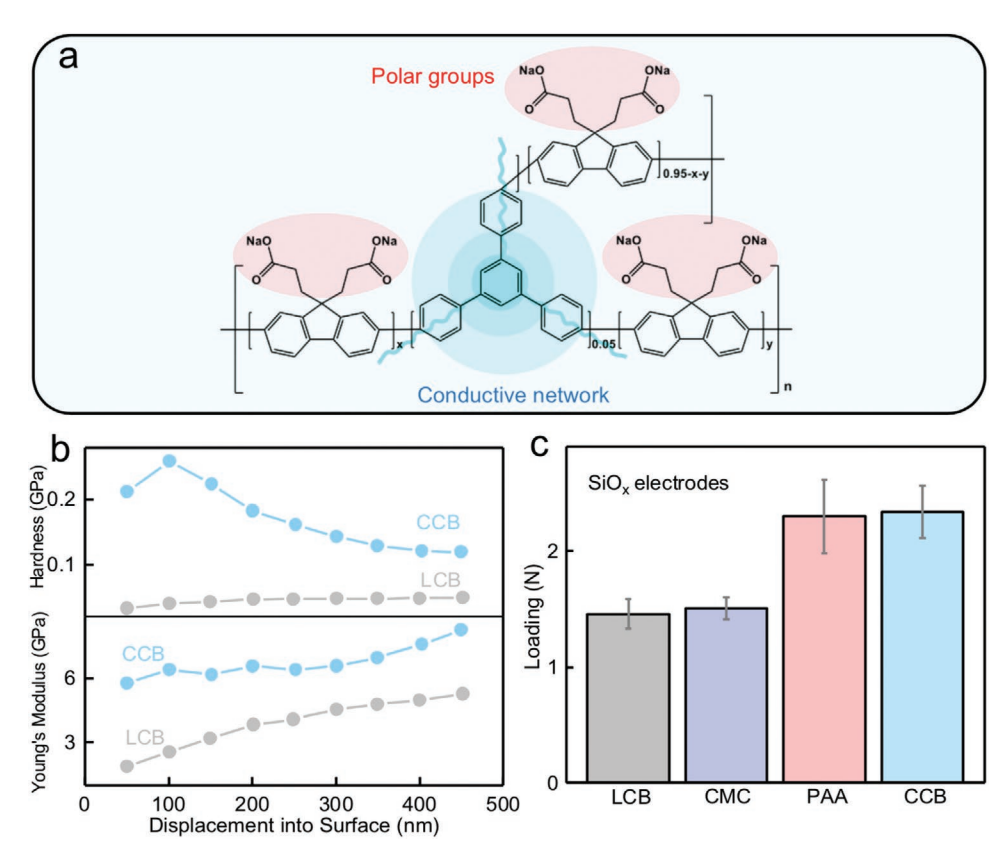


Figure 1. a) Structure of the polyfluorene-type cross-linked conductive binder abbreviated as CCB. b) Hardness and Young's modulus of polymer films obtained from the nanoindentation test. c) Adhesion force of SiO_x/LCB, SiO_x/CMC, SiO_x/PAA, and SiO_x/CCB electrodes.

around 1706 cm⁻¹ corresponding to the stretching vibration of carbonyl group appears when CCB is mixed with SiO_x particles in the slurry and treated at 135 °C for 12 h, indicating the formation of new chemical bonds (CO-OR) between the polymer and SiO_x particles. [26,27] Additionally, the SiO_x/CCB electrode was analyzed by X-ray photoelectron spectroscopy (XPS). The C1s XPS spectra of the CCB (Figure S10, Supporting Information) show a clear peak corresponding to -COONa functional groups at 288.1 eV, which shifts to 288.8 eV (-C = O-(OR)) when prepared into electrodes with SiOx, indicating the formation of chemical bonds between binder and active materials. Both results reveal the strong chemical interaction between the polar groups on the SiO_x surface and CCB moieties. Therefore, it can be concluded that both the cross-linked backbone and the functionalized side chains collectively contribute to the excellent mechanical properties of CCB.

Next, the electronic conductivity of CCB and LCB is measured to be 5.5×10^{-2} and 3.4×10^{-2} S cm⁻¹, respectively, using direct current 4-prober method. These values are 6-9 orders higher than those of conventional binders reported previously (Figure 2a).[35] In addition, the polymer backbone can be catholically doped for enhanced electric conductivity under the reducing environment. Figure 2b shows the calculated highestoccupied molecular orbital (HOMO) and lowest-unoccupied molecular orbital (LUMO) molecular orbitals distribution for both initial state and reduced state of the CCB segments. Note that sodium ions in the polymer can be readily substituted with lithium ions in the electrolyte which could potentially boost the transfer efficiency of lithium ions. [36–39] The band gap decreases from 6.158 to 1.898 eV after the reduction process, resulting in enhanced electronic conductivity. Improved conductivity is further verified by the impedance measurements (Figure S11, Supporting Information). A Randles circuit is used to fit the results with R_s as the electrolyte resistance and $R_{\rm ct}$ as the charge-transfer resistance. It is clearly observed that the $R_{\rm ct}$ of CCB decreases from 399.4 to 257.6 Ω by negatively scanning the potential from 1 to 0.5 V (vs Li/Li⁺). The R_{ct} of CCB remains almost unchanged when the potential is swept to 0.01 V (vs Li/Li+), indicating no further n-type doping within this voltage range. More importantly, as shown in Figure 2c, in the absence of conductive carbon, the high conductivity of CCB results in a lower volume resistivity of SiO_x/CCB electrode compared to SiO_x/PAA and SiO_x/CMC. From above, it can be concluded that CCB not only inherits excellent conductivity and n-type doping ability from LCB but also serves as a more robust secondary conductive network owing to its superior mechanical properties over LCB. The role of secondary conductive network in SiO_x anodes is illustrated in Figure 2d,e: As a soft matrix, CCB greatly extends the conductive network within the electrode via molecular-level contact with particles and provides a greater contact area. As a result, current distribution on particle surface is more uniform compared to that using non-conductive binders, achieving electronic depolarization effect.^[40]

The galvanostatic cycling tests of SiO_x electrodes using different binders are then carried out to evaluate their electrochemical performance. The role of binders' electronic conductivity is

16136829, 2021, 42, Downloaded from https://onlinelbtary.wiley.com/doi/10.1002/snlll.20210256 by University Town Of Shenzhen, Wiley Online Library on [26111025]. See the Terms and Conditions (https://onlinelibrary.wiley.com/terms-and-onditions) on Wiley Online Library for rules of use; OA articles are governed by the applicable Creative Commons Licenses

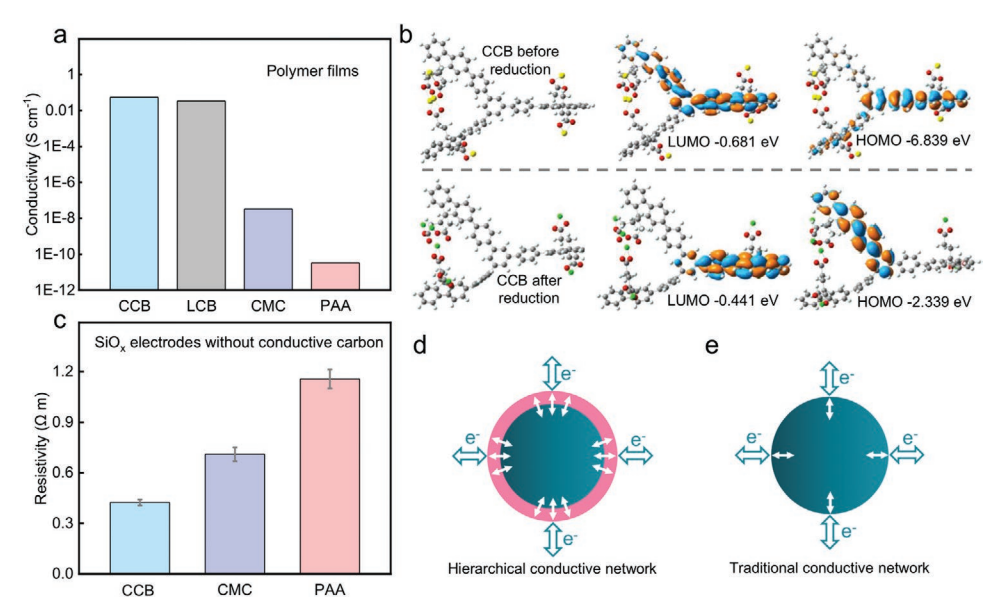


Figure 2. a) Electronic conductivity of CCB, LCB, CMC, and PAA. b) Molecular structures and molecular frontier orbitals of initial state and reduced state of CCB segments. c) Resistivity of SiO_v/CCB, SiO_v/CMC, and SiO_v/PAA electrodes in the absence of conductive carbon. d) Scheme of SiO_v electrodes with secondary conductive network during cycling. e) Scheme of SiO_x electrodes without secondary conductive network during cycling.

first estimated through rate performance tests (Figure 3a). It is shown that SiO_x/CCB delivers best rate capability, followed by SiO_x/LCB. This result could be attributed to the existence of secondary conductive network, which shows excellent depolarization effect under high current densities. It is noteworthy that the superior rate performance of SiO_x/CCB over SiO_x/LCB is mainly due to the better mechanical properties of CCB. To further demonstrate this concept, SiO_x anodes using different binders were also prepared without any conductive carbon. The cycling performance (Figure 3b) clearly shows that in the absence of primary conductive network, SiO_x electrodes using PAA and CMC are almost electrochemically inert which gives rise to the "death" of electrodes. By contrast, only the electrode using LCB and CCB exhibits acceptable initial capacity and capacity retention over 50 cycles. Since the electronic conductivity of LCB and CCB are almost the same, the enhanced performance of CCB over LCB can be attributed to its better mechanical strength. This result strongly confirms the critical role of secondary conductive network: Not only facilitating fast electron exchange at the interface of micro-sized SiO_x during charge/discharge, but also allowing electrons to travel through the electrode. Same conclusions can be drawn from the rate performance of cells above (Figure S12, Supporting Information), where only SiO_x/CCB is able to be charged and discharged properly. Next, the cycling performances of different binders are also evaluated at the current density of 0.4 A g⁻¹ (Figure 3c). The initial capacity of SiO_x/CCB is the highest, suggesting that the molecular level contact between SiO_x and the conductive network, as well as, the superior mechanical properties of CCB are able to drain more capacity from the micro-sized active materials. An initial specific capacity of 1318 mAh g⁻¹ is achieved for SiO_x/CCB, which is equivalent to a specific areal capacity over 2.5 mAh cm⁻². After 100 cycles, the capacity of SiO_x/CCB barely fades (1283 mAh g⁻¹, 97.3%)

at 0.4 A g⁻¹, which outperforms SiO_x/CMC (56.7% capacity retention) and SiO_x/PAA (72.9% capacity retention). Even after 250 cycles, the specific areal capacity can be maintained above 2.1 mAh cm⁻² (Figure S13, Supporting Information). Despite the slightly lower initial capacity, SiO_x/LCB also exhibits a high capacity retention owing to the effectiveness of secondary conductive network, but the unstable cycling curve indicates the insufficient mechanical strength of LCB. The results shown above suggest that under relatively low current densities, the robustness of secondary conductive network does not vet seem to be a key factor. In addition, despite exhibiting an inferior initial coulombic efficiency of 67.6%, SiOx/CCB exhibits a muchimproved coulombic efficiency (CE) above 99% compared to the other electrodes during subsequent cycles which demonstrates the best integrity and stability of SiOx/CCB (Figure S14, Supporting Information). From the potential profiles of different cells after 100 cycles (Figure 3d), it can be clearly seen that the capacity fading of SiOx/PAA and SiOx/CMC are accompanied with large over-potentials, suggesting a disrupted conductive network. However, by increasing the current density to 0.8 A g⁻¹ (Figure 3e), the cycling stability of SiO_x/LCB significantly drops (86.3% after 110 cycles) while a high capacity retention can still be achieved for SiO_x/CCB (88.1% after 250 cycles). The large overpotential discrepancy between SiO_x/CCB and SiO_x/LCB at 100th cycle (Figure S15, Supporting Information) also indicates that a mechanically stronger binder is necessary to maintain the integrity of the micro-sized SiO_x electrodes especially at a high rate owing to the more rapid volume variation of active materials. With the help of CCB, excellent cycling performance has been achieved for micro-sized SiOx anodes when compared with previous studies (Table S1, Supporting Information). Despite exhibiting good electronic conductivity and desirable mechanical properties, the large-scale production of CCB remains an issue, which shall be addressed in the future.

16136829, 2021, 42, Downloaded from https:

nelibrary.wiley.com/doi/10.1002/smll.202102256 by University Town Of Shenzhen, Wiley Online Library on [26/11/2025]. See the Terms

nditions) on Wiley Online Library for rules of use; OA articles are governed by the applicable Creative Commons License

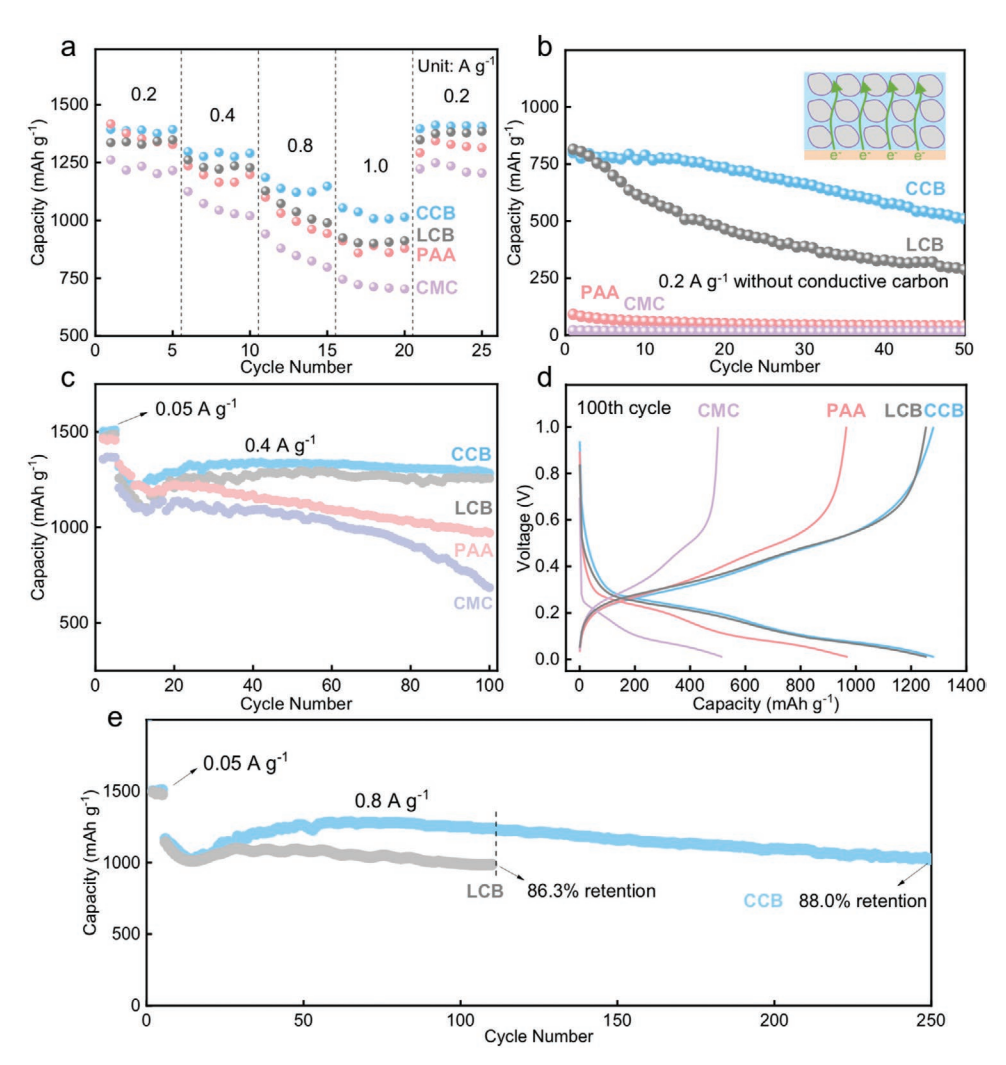


Figure 3. a) Rate performance of SiO_x electrodes using different binders at a current density of 0.2, 0.4, 0.8, and 1.0 A g^{-1} after 5 cycles at a rate of 0.05 A g^{-1} . b) Cycling performance of SiO_x electrodes using different binders in the absence of conductive carbon at a current density of 0.2 A g^{-1} after 5 cycles at a rate of 0.05 A g^{-1} . c) Cycling performance and d) the corresponding voltage profiles of 100th cycle of SiO_x electrodes using different binders at a current density of 0.4 A g^{-1} . e) Cycling performance of SiO_x electrodes using different binders at a current density of 0.8 A g^{-1} .

Furthermore, full cells with LiFePO $_4$ cathode and SiO $_x$ /CCB anode were assembled and tested. As shown in Figure S16, Supporting Information, a stable specific capacity of 140 mA g $^{-1}$ can be achieved for the full cell which exhibits the outstanding performance of CCB.

To further investigate the impact of CCB in SiO_x electrodes, scanning electron microscope (SEM) was used in combined with focused ion beam (FIB) to observe both surface and interior morphology of SiO_x electrodes before and after 100 cycles at 0.4 A g⁻¹. It can be observed that the surface morphology of SiO_x/CCB is perfectly constructed without any crack (**Figure 4a**), which is beneficial for minimizing polarizations; whereas SiO_x/LCB (Figure 4b), SiO_x/PAA (Figure 4c), and SiO_x/CMC (Figure 4d) all exhibit various degrees of fracture. Despite the strong adhesive force of PAA, SiO_x/PAA electrode suffers from obvious fractures owing to the lack of ductility for PAA to adapt to deformations, which causes severe stress concentration. Therefore, fractures will form at the relatively weak spots and

develop subsequently. By contrast, exhibiting a lower hardness and a moderate Young's modulus, CCB facilitates better electrode integrity, which points out a new potential direction for binder design. After 100 cycles, the surface of SiO_x/CCB was well preserved without obvious fracture (Figure 4e). By sharp contrasts, the surface morphology of other electrodes deteriorates in different ways: numerous micro-cracks have emerged in SiO_x/LCB (Figure 4f); cracks in SiO_x/PAA have extended markedly during cycling (Figure 4g); the structure of SiO_x/CMC become loosened without showing deep fractures (Figure 4h). In addition to the top-view SEM images, cross-sectional SEM images provide a different angle to observe the electrode structures. From Figure 4i, it can be clearly observed that cycled SiO_x/CCB exhibit minimum interior cracks, which agrees with Figure 4e. Therefore, electrons could freely transfer within the electrode. As for SiO_x/LCB (Figure 4j), the main structure remains intact by and large although some micro-cracks can be observed, indicating that mechanically the electrode is on

Figure 4. Top-view SEM images of SiO $_x$ /CCB, SiO $_x$ /PAA, and SiO $_x$ /CMC a–d) before and e–h) after 100 cycles at a current density of 0.4 A g $^{-1}$, respectively. Cross-sectional SEM images of i) SiO $_x$ /CCB, j) SiO $_x$ /LCB, k) SiO $_x$ /PAA, and l) SiO $_x$ /CMC after 100 cycles at a rate of 0.4 A g $^{-1}$. The scale bar represents 50 μ m.

the verge of collapse. This explains its relatively good electrochemical performance at 0.4 A g⁻¹ and a poorer one at 0.8 A g⁻¹. Despite the highest hardness and Young's modulus of PAA among the binders, SiOx/PAA seems to suffer from more severe fractures. Although the abundant -COOH groups of PAA could firmly hold SiO_x particles together in a local area, the stress originated from the volume change could not be relieved due to the excessive stiffness of PAA which proves that a moderate mechanical strength is preferred. From the numerous interior voids developed within SiO_x/CMC (Figure 4l), it can be inferred that the electrode suffers from severe disengage of active materials which can well explain the rapid capacity decrease owing to the lack of adhesion and poor mechanical strength of CMC. In addition, the thicknesses of electrodes of SiO_x/CCB and SiO_x/LCB with the same mass loading were 34 and 55 µm, respectively (Figure S17, Supporting Information), after 250 cycles at 0.8 A g⁻¹, showing suppressing effect of CCB on volume expansion of electrodes. As a conclusion, disintegration of electrodes or pulverization of active materials could physically tear apart the conducting network hence become the origin of the capacity fading and the increase of over-potential.

Exhibiting moderate mechanical strength and excellent electrochemical properties, CCB facilitates well-preserved electrode structures. To better demonstrate this claim, the stress distribution on the surface of SiO_x particles during cycling is simulated by solving partial differential equations and the finite element method (Figure S18, Supporting Information). It is shown that in the presence of binder with high electronic conductivity, the surface stress of SiO_x is lower than traditional non-conductive binder regardless of Young's modulus, demonstrating that the existence of secondary conductive network has a good effect on reducing surface stress on SiO_x particles during cycling.

3. Conclusion

In this study, a CCB is designed to tackle the cycling issues of micro-sized SiO_x material from two aspects: 1) Exhibiting high electronic conductivity, CCB serves as an adaptive secondary conductive network in addition to the stiff primary conductive network, facilitating faster interfacial charge transfer processes

www.small-journal.com

for micro-sized SiO_x in the molecular level; 2) the cross-linked structure of CCB shows resilient mechanical properties, enabling the electrode to endure deformation after prolonged cycling. Consequently, owing to the use of CCB, the hierarchical conductive network within SiO_x anode is well preserved during long-term cycling, achieving excellent electrochemical performance. The above results reveal a promising binder for Sibased materials which unite good conductivity with resilient mechanical properties.

4. Experimental Section

Materials: 1,3,5-Tris (4-bromophenyl) benzene was purchased from Aladdin. Other chemicals for synthesis of polymers were purchased from Innochem, and the tetrahydrofuran (THF) was distilled in the presence of Na with benzophenone. The compounds M1 and M2 and the polymer poly[9,9-bis (3-propanoate) fluorene] (LCB) were synthesized according to the literature. [24] Micro-sized SiO_x was kindly provided by Shenzhen Dajiabang Co. LTD. Freshly deionized water was used in experiments. The electrolyte was obtained from DoDoChem (Suzhou, China).

Synthesis of Cross-Linked Conductive Binder-Bu: A mixture of 2,7-dibromo-9,9-bis(3-(tert-butyl propanoate))fluorene (M1) (2.477 g, 4.2675 mmol), 2,7-bis(4,4,5,5-tetramethyl-1,3,2-dioxaborolan-2-yl)-9,9-bis(3-(tert-butyl propanoate))fluorene (M2) (3.372 g, 5 mmol), 1,3,5-tris(4-bromophenyl)benzene (M3) (0.2648 g, 0.4875 mmol), tetrakis(triphenylphosphine)palladium (0.1733 g, 0.15 mmol), and several drops of Aliquat 336 were placed in a Schlenk flask. Distilled THF (48 mL) and Na₂CO₃ (16 mL, 2 mol L⁻¹) were added at Ar atmosphere. The mixture was stirred vigorously at 85 °C for 72 h. After the mixture was cooled down, the polymer was precipitated from dichloromethane three times, filtered, and dried under vacuum, resulting in an 83% yield.

Synthesis of Cross-Linked Conductive Binder: CCB-Bu (1.5 g) was dissolved in dichloromethane solution with 15 wt% trifluoroacetic acid (60 g). The mixture was stirred 12 h at room temperature. After the reaction stopped, the solvent was removed under reduced pressure, yielding a yellow residue. The residue was treated with aqueous NaOH solution (1 mol L⁻¹) and purified by dialysis against deionized water for 3 days. The purified solution was free-dried to give CCB with 72% yield.

Material Characterizations: The top-view morphology characterization of as-prepared samples was conducted using field-emission scanning electron microscopy (ZEISS SUPRA55, Carl Zeiss). The cross-section images of the electrodes were obtained using FEI (Scios) equipment. For the analysis of cycled electrodes, coin-cells were disassembled in an argon-filled glove box. The electrodes were washed with DMC, followed by drying under vacuum for 3 h. FTIR spectra were collected on a Nicolet Avatar 360 spectrophotometer (ATR). XPS were collected by ESCALAB 250Xi. For XPS measurements, the SiO_x/CCB electrodes without conductive carbon were dried at 135 °C in the vacuum oven for 12 h, then washed by deionized water to expose the surface of SiOx and dried for the second time. The hardness and Young's Modulus were measured on an Agilent G200 Nano Indenter. The thickness of the polymer films was measured with a Bruker Dektak XT stylus profiler. The conductivities of polymer films were measured using Keithley 4200-SCS semiconductor characterization system and probe station (PS-100, Lakeshore) at room temperature in ambient air. Before measurements of electric conductivity, four gold electrodes (2 mm \times 2 mm) were vacuum-deposited onto the surface of the polymer thin films. The distance between two gold electrodes was 5 mm. The conductivities were measured with a fourprobe method, and calculated from their measured sheet resistances and exact film thickness. The internal resistance (AC-IR) of electrodes was measured using HIOKI 3561 battery HiTester. The electrode plate with a diameter of 4 cm was gripped by a pair of coppery terminals with a diameter of 3.5 cm for 30 s during testing under a pressure of 10 MPa. The thickness of plates was obtained by a micrometer caliper. The volume resistivity was calculated through the formula $\rho = RS/L$.

Three plates of each electrode were tested and the mean value and the standard deviation was demonstrated.

Adhesion Test: Adhesion test of the SiO_x electrodes were conducted on a microcomputer controlled electronic universal testing machine (MDTC-EQ-M12-01). The electrode samples were cropped to strips of 20 × 60 mm and both sides of the samples were attached to 3M 600 Scotch tapes (20 mm in width) with one end open. The machine grips were attached to the free ends of 3M tapes. The electrodes were peeled off the copper current collector by pulling the Scotch tapes at the angle of 180° at a constant displacement rate of 60 mm min $^{-1}$. The applied force was continuously measured and the plateau values of force were collected.

Preparation of Electrodes: The electrodes were made by a typical slurry casting method with active materials (SiO_x), conductive carbon (acetylene black), and binder (CCB, LCB, PAA, or CMC) at a mass ratio of 8:1:1. The slurry was casted onto a Cu foil and dried at room temperature, then it was pressed by a roller. The electrodes were dried at 135 °C under vacuum and cut into disks with a diameter of 10 mm. The typical mass loading of active materials was between 1.9 and 2.1 mg cm⁻². The electrodes without any conductive carbon were prepared by using the same procedure with a typical mass loading of active materials of 1 mg cm⁻². Two-electrode CR2032 coin-type half-cells were assembled in an argon-filled glove box with lithium foils as the counter electrodes. The electrolyte was 1.0 M LiPF₆ in 1:1 (v/v) EC/DEC with 10% FEC and the separator was porous PP films (Celgard 2400). The full cell was designed with a N/P ration of ≈1.2. The anodes were discharged and charged 5 cycles before use. The lithium iron phosphate (LFP) cathode electrodes (Canrd) were dried in vacuum at 80 °C for 2 h before use. Coin-type full cells with the LFP cathodes and SiO_x anodes were assembled using same electrolytes and separators as those used in the half cells.

Electrochemical Measurements: The cycling and rate capability tests were carried out using a Neware battery test system within the voltage range of 2.5–4.2 V (vs Li/Li⁺) for the full cells and 0.01–1 V (vs Li/Li⁺) for the half cells. EIS experiments were performed on a CHI604E electrochemical station with a frequency range of 1 MHz to 1 Hz. Unless otherwise specified, all electrochemical measurements were conducted at room temperature in half cells, as well as, the annotated cycling conditions.

Calculation Details: All calculations were based on the Gaussian 09 package^[41] with the density functional theory method. The m062x/6-31+G(d) theory level was used to optimize the molecular structure and perform frequency analysis. The 6–31+G(d) basis was used for the C, O, H, Na, and Li atoms. The calculated HOMO and LUMO were shown in the GaussView6.0 software.

Supporting Information

Supporting Information is available from the Wiley Online Library or from the author.

Acknowledgements

This work was financially supported by the National Key R&D Program of China (2016YFB0700600), China Postdoctoral Science Foundation (2019M660317), Shenzhen Science and Technology Program (Grant No. RCBS20200714114820077).

Conflict of Interest

The authors declare no conflict of interest.

Data Availability Statement

Research data are not shared.

www.advancedsciencenews.com



16136829, 2021, 42, Downloaded from https://onlinelibrary.wiley.com/doi/10.1002/smll.202102256 by University Town Of Shenzhen, Wiley Online Library on [26/11/2025]. See the Terms and Conditions (https://onlinelibrary.wiley.com/terms

-and-conditions) on Wiley Online Library for rules of use; OA articles are governed by the applicable Creative Commons License

Keywords

conductive binder, cycle stability, lithium-ion batteries, polymer design, SiO_{\star} anode

Received: April 19, 2021 Revised: July 2, 2021 Published online: September 15, 2021

- [1] M. Armand, Nature 2001, 414, 359.
- [2] S. Yang, R. He, Z. Zhang, Y. Cao, X. Gao, X. Liu, Matter 2020, 3, 27.
- [3] L. Yang, K. Yang, J. Zheng, K. Xu, K. Amine, F. Pan, Chem. Soc. Rev. 2020, 49, 4667.
- [4] J. Zheng, Y. Ye, F. Pan, Natl. Sci. Rev. 2019, 2, 242.
- [5] H. Wu, Y. Cui, Nano Today 2012, 7, 414.
- [6] C. K. Chan, H. Peng, G. Liu, K. McIlwrath, X. F. Zhang, R. A. Huggins, Y. Cui, Nat. Nanotechnol. 2008, 3, 31.
- [7] S. W. Lee, M. T. McDowell, J. W. Choi, Y. Cui, Nano Lett. 2011, 11, 3034.
- [8] Z. Liu, Q. Yu, Y. Zhao, R. He, M. Xu, S. Feng, S. Li, L. Zhou, L. Mai, Chem. Soc. Rev. 2019, 48, 285.
- [9] H. Xue, Y. Wu, Y. Zou, Y. Shen, G. Liu, Q. Li, D. Yin, L. Wang, J. Ming, Adv. Funct. Mater. 2020, 30, 1910657.
- [10] H. Ming, J. Qiu, S. Zhang, M. Li, X. Zhu, L. Wang, J. Ming, ChemElectroChem 2017, 4, 1165.
- [11] Y. Shen, Z. Cao, Y. Wu, Y. Cheng, H. Xue, Y. Zou, G. Liu, D. Yin, L. Cavallo, L. Wang, J. Ming, J. Mater. Chem. A 2020, 8, 12306.
- [12] J. W. Choi, D. Aurbach, Nat. Rev. Mater. 2016, 1, 16013.
- [13] J. Y. Li, Q. Xu, G. Li, Y. X. Yin, L. J. Wan, Y. G. Guo, Mater. Chem. Front. 2017, 1, 1691
- [14] S. Komaba, K. Shimomura, N. Yabuuchi, T. Ozeki, H. Yui, K. Konno, J. Phys. Chem. C 2011, 115, 13487.
- [15] Y. Cho, J. Kim, A. Elabd, S. Choi, K. Park, T.-w. Kwon, J. Lee, K. Char, A. Coskun, J. W. Choi, Adv. Mater. 2019, 31, 1905048.
- [16] T. Kang, J. Chen, Y. Cui, Z. Wang, H. Xu, Z. Ma, X. Zuo, X. Xiao, J. Nan, ACS Appl. Mater. Interfaces 2019, 11, 26038.
- [17] S. Wu, Y. Yang, C. Liu, T. Liu, Y. Zhang, B. Zhang, D. Luo, F. Pan,
 Z. Lin, ACS Energy Lett. 2021, 6, 290.
- [18] H. Chen, M. Ling, L. Hencz, H. Y. Ling, G. Li, Z. Lin, G. Liu, S. Zhang, Chem. Rev. 2018, 118, 8936.
- [19] G. Liu, S. Xun, N. Vukmirovic, X. Song, P. Olalde-Velasco, H. Zheng,
- V. S. Battaglia, L. Wang, W. Yang, *Adv. Mater.* **2011**, *23*, 4679. [20] S. J. Park, H. Zhao, G. Ai, C. Wang, X. Song, N. Yuca, V. S. Battaglia,
- [20] S. J. Park, H. Zhao, G. Al, C. Wang, X. Song, N. Yuca, V. S. Battaglia W. Yang, G. Liu, *J. Am. Chem. Soc.* **2015**, *137*, 2565.
- [21] T. M. Higgins, S. H. Park, P. J. King, C. Zhang, N. McEvoy, N. C. Berner, D. Daly, A. Shmeliov, U. Khan, G. Duesberg, V. Nicolosi, J. N. Coleman, ACS Nano 2016, 10, 3702.

- [22] H. Zhao, Z. Wang, P. Lu, M. Jiang, F. Shi, X. Song, Z. Zheng, X. Zhou, Y. Fu, G. Abdelbast, X. Xiao, Z. Liu, V. S. Battaglia, K. Zaghib, G. Liu, Nano Lett. 2014, 14, 6704.
- [23] H. Zhao, N. Yuca, Z. Zheng, Y. Fu, V. S. Battaglia, G. Abdelbast, K. Zaghib, G. Liu, ACS Appl. Mater. Interfaces 2015, 7, 862.
- [24] D. Liu, Y. Zhao, R. Tan, L. L. Tian, Y. Liu, H. Chen, F. Pan, Nano Energy 2017, 36, 206.
- [25] Y. Zhao, L. Yang, Y. Zuo, Z. Song, F. Liu, K. Li, F. Pan, ACS Appl. Mater. Interfaces 2018, 10, 27795.
- [26] B. Koo, H. Kim, Y. Cho, K. T. Lee, N. S. Choi, J. Cho, Angew. Chem., Int. Ed. 2012, 51, 8762.
- [27] J. Song, M. Zhou, R. Yi, T. Xu, M. L. Gordin, D. Tang, Z. Yu, M. Regula, D. Wang, Adv. Funct. Mater. 2014, 24, 5904.
- [28] S. Sun, D. He, P. Li, Y. Liu, Q. Wan, Q. Tan, Z. Liu, F. An, G. Gong, X. Qu, J. Power Sources 2020, 454, 227907.
- [29] S. Jiang, B. Hu, Z. Shi, W. Chen, Z. Zhang, L. Zhang, Adv. Funct. Mater. 2020, 30, 1.
- [30] S. Choi, T. woo Kwon, A. Coskun, J. W. Choi, Science 2017, 357, 279.
- [31] X. Wang, S. Liu, Y. Zhang, H. Wang, A. A. Aboalhassan, G. Li, G. Xu, C. Xue, J. Yu, J. Yan, B. Ding, ACS Appl. Mater. Interfaces 2020, 12, 28122
- [32] L. Wang, T. Liu, X. Peng, W. Zeng, Z. Jin, W. Tian, B. Gao, Y. Zhou, P. K. Chu, K. Huo, Adv. Funct. Mater. 2018, 28, 1704858.
- [33] R. Qin, Y. Wang, M. Zhang, Y. Wang, S. Ding, A. Song, H. Yi, L. Yang, Y. Song, Y. Cui, J. Liu, Z. Wang, S. Li, Q. Zhao, F. Pan, *Nano Energy* 2021, 80, 105478.
- [34] Y. Wang, Y. Wang, C. Chen, X. Chen, Q. Zhao, L. Yang, L. Yao, R. Qin, H. Wu, Z. Jiang, F. Pan, Chem. Commun. 2021, 57, 5326.
- [35] K. L. Wang, K. T. Chen, Y. H. Yi, Y. H. Hung, H. Y. Tuan, M. Horie, ACS Sustainable Chem. Eng. 2020, 8, 1043.
- [36] Z. Li, Y. Zhang, T. Liu, X. Gao, S. Li, M. Ling, C. Liang, J. Zheng, Z. Lin, Adv. Energy Mater. 2020, 10, 1903110.
- [37] L. Qiu, Z. Shao, M. Yang, W. Wang, F. Wang, J. Wan, J. Wang, Y. Bi, H. Duan, Cellulose 2014, 21, 615.
- [38] J. Li, D. B. Le, P. P. Ferguson, J. R. Dahn, Electrochim. Acta 2010, 55, 2991
- [39] R. R. Garsuch, D.-B. Le, A. Garsuch, J. Li, S. Wang, A. Farooq, J. R. Dahn, J. Electrochem. Soc. 2008, 155, A721.
- [40] W. Ren, K. Wang, J. Yang, R. Tan, J. Hu, H. Guo, Y. Duan, J. Zheng, Y. Lin, F. Pan, J. Power Sources 2016, 331, 232.
- [41] M. J. Frisch, G. W. Trucks, H. B. Schlegel, G. E. Scuseria, M. A. Robb, J. R. Cheeseman, G. Scalmani, V. Barone, G. A. Petersson, H. Nakatsuji, X. Li, M. Caricato, A. Marenich, J. Bloino, B. G. Janesko, R. Gomperts, B. Mennucci, H. P. Hratchian, J. V. Ortiz, A. F. Izmaylov, J. L. Sonnenberg, D. Williams-Young, F. Ding, F. Lipparini, F. Egidi, J. Goings, B. Peng, A. Petrone, T. Henderson, D. Ranasinghe, et al., Gaussian 09, Revision A.02, Gaussian Inc., Wallingford, CT 2016.